Force Actuated Real-Time Hybrid Model Testing of a Moored Vessel: A Case Study Investigating Force Errors ⋆

Einar S. Ueland* Roger Skjetne Stefan A. Vilsen *****

*/**/*** *Centre for Autonomous Marine Operations and Systems; Norwegian University of Science and Technology (NTNU AMOS); Department of Marine Technology; NO-7491 Trondheim, Norway*
**Corresponding author: einar.s.ueland@ntnu.no*
****SINTEF Ocean;, NO-7465 Trondheim, Norway*

Abstract: This paper presents a study where real-time hybrid testing is used to emulate a moored barge. The barge is modelled physically while the mooring forces are simulated numerically and actuated onto the physical substructure. Assuming no errors in modelling of the numerical substructure, we investigate what separates the instantaneous forces acting on the physical substructure, from the forces that would be acting on it in the ideal, non-substructured case that we are trying to replicate. Four different types of errors are identified, discussed, and partly quantified.

Keywords: Force control, Hybrid Testing, Error analysis, Sub-structuring, Mooring systems.

1. INTRODUCTION

Real-time hybrid model testing (or *ReaTHM® testing* [1]) is an experimental method for performing hydrodynamic model-scale testing, where systems/structures are partitioned into physical and numerical substructures. The physical substructure is then modelled physically in a laboratory facility, while the numerical substructure is modelled numerically using simulation software. The two are then coupled in real-time using a measurement and control-system interface. In general, we want to perform model-scale testing to identify the characteristics and responses of structures. This is motivated by the fact that complex hydrodynamic phenomena are difficult to model numerically or analytically. Real-time hybrid model testing is an extension to conventional model-scale testing, in that it enables the inclusion of numerically simulated components, into the classical experimental regime. As such the method can address some of the challenges and limitations of traditional model testing, which due to the complexity of structures, limitations of facilities, demand for rapid prototyping, or conflicts from differences in scaling effects, is not always feasible or practical to perform on the whole structure.

One application of ReaTHM, hereafter simply referred to as hybrid testing, is to use it in the testing of moored systems, where (in particular for deep-water structures) the spacial limitation of the basin-infrastructure is identified as a major challenge (Stansberg et al., 2002). In Cao and Tahchiev (2013) and Sauder et al. (2018) the use of hybrid testing for active mooring line truncation has been studied through numerical simulations. In these cases, the flexibility of the mooring lines means that imposing target displacements on the physical substructure is an alternative. This is what is typically done in seismic engineering, where hybrid testing has been studied extensively (Carrion, 2007).

In the approach seen in this paper, as also studied by Vilsen et al. (2017), the entirety of the mooring lines are modelled numerically, meaning that sub-structuring is performed at the fairled point connecting the mooring system to the floating structure. Since the interface of the numerically calculated effort, in this case, is directly on the rigid body under study, we need to (in order to maintain flexibility) actuate target-forces, rather than displacements, on the floating test structure.

In this paper, a ship-shaped vessel is tested using the hybrid testing strategy. To the author's knowledge, this is the first time hybrid testing has been applied to ship-shaped vessels. In the present work, the focus is on developing the hybrid testing concept, rather than quantifying the responses of the moored structure. If the goal, instead, were to reproduce the real-world mooring system accurately, one would typically use a model of a full-scale vessel, in combination with a high fidelity numerical simulation tool for the mooring system. See for example Vilsen et al. (2017).

The main focus is on the investigation of issues relating to force control. In a broader sense, the objective of the presented work is to further develop the experimental framework of hybrid testing (building of the work of Vilsen et al. (2018)). The long-term goal is for hybrid testing to become a qualified method, which is accepted and valued by industrial stakeholders.

⋆ This work was supported by the Research Council of Norway through the Centre of Excellence AMOS, project no. 223254, and through grant No. 254845/O80 "Real-Time Hybrid Model Testing for Extreme Marine Environments".

[1] *ReaTHM® testing* is a registered trademark of SINTEF Ocean.

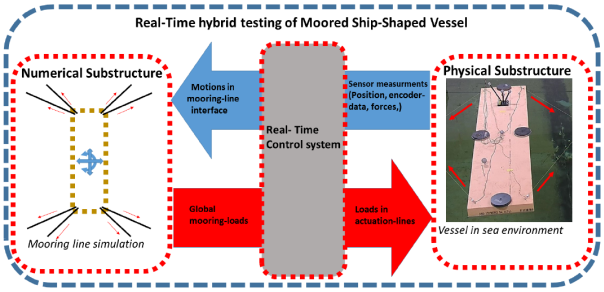

Fig. 1. The real-time hybrid test loop for hybrid testing of a ship-shaped vessel, where mooring lines are numerically simulated. Right image is from the actual test setup.

1.1 Real-Time Hybrid Test-Loop

The numerical and physical substructures are coupled through the real-time hybrid test loop as illustrated in Figure 1. The goal is to replicate the responses of the ideal non-substructured system in terms of relevant performance measures (often referred to as key performance indicators), when exposed to relevant loads. Based on measured responses of the physical structure, the numerical substructure calculates and outputs target forces to be applied to the physical substructure.

1.2 Problem Statement

Assuming no modeling errors of the numerical substructure, we are asking the following question: what distinguish the loads acting on the physical substructure in a hybrid test setup from the ideal loads that would be acting on it in the real non-substructured system that we try to replicate?

We aim to identify (and partly quantify) discrepancies related to force control in a real-time hybrid test setup. Using experiences from the test-case, we identify four error sources that are studied and discussed:

(1) Force allocation errors.
(2) Force estimation errors.
(3) Target-force tracking errors
(4) Delay-induced force errors.

2. EXPERIMENTAL SETUP AND METHODS

2.1 Experimental Setup

A ship-shaped structure in the form of a barge was set up in an experiment to test various objectives related to hybrid model testing; see Figure 1. The tests were performed in a basin laboratory at NTNU (MC-Lab). This is equipped with a camera tracking system that measures the local position and attitude of the vessel.

Physical Substructure For geometric simplicity and being easy to handle, the barge seen in Figure 2 was chosen as the physical substructure. Relevant dimensions are listed in Table 1. Ballasted with weights, the mass of the barge was about 15.35 kg

Numerical Substructure A linear mooring model with target-forces proportional to the excursion in position

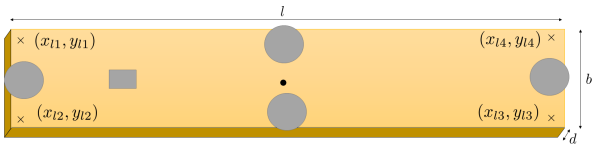

Fig. 2. Barge dimensions. Corresponding data in Table 1.

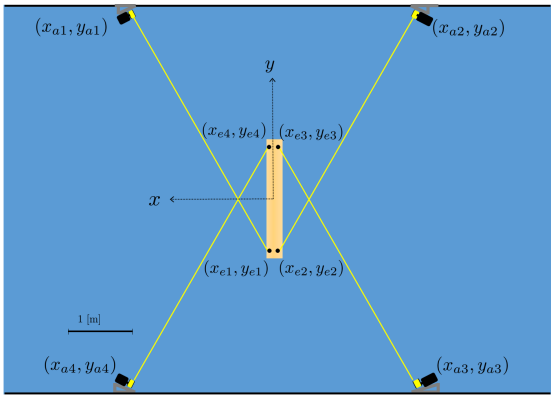

Fig. 3. Barge and actuator configuration when barge is centred in origo.

Table 1. Test-dimensions and placements

	Distance/Position [m]
l, b, d	(2.0 , 0.45 , 0.085)
$\boldsymbol{x}_{a1}, \boldsymbol{x}_{a2}, \boldsymbol{x}_{a3}, \boldsymbol{x}_{a4}$	$(x\ ,\ y) : (\pm 3.25\ ,\ \pm 2.6)$
$\boldsymbol{x}_{l1}, \boldsymbol{x}_{l2}, \boldsymbol{x}_{l3}, \boldsymbol{x}_{l4}$	$(x\ ,\ y) : (\pm 0.175\ ,\ \pm 0.95)$

and heading (i.e., x, y, ψ) was chosen as the numerical substructure. This means that the numerical substructure is a linear approximation to a horizontal mooring model:

$$F_t = -\left[k_x x \ k_y y \ k_\psi \psi\right]^T + \boldsymbol{\omega}, \tag{1}$$

where F_t is the target interface force-vector, k_x, k_y and k_ψ are linear stiffness coefficients, and $\boldsymbol{\omega} = [\omega_x \ \omega_y \ \omega_\psi]^T$ represents additional artificial environmental loads we may subject the structure to.

Actuators, Placement, and Control Forces are actuated using four separate actuators connected to the floating structure through thin braided lines. The actuators are similar to those described by Ueland and Skjetne (2017), consisting of a DC-motor connected, via a clock spring and a line, to the end-effector on the physical structure. The basin walls where the actuators could be placed, is of limited dimensions. Therefore, in order to have a flexible system, capable of applying relevant loads, the symmetric cross configuration illustrated in Figure 3 was chosen. The positions of the actuators and end-effectors are listed in Table 1.

The control system is similar to that of Vilsen et al. (2018). Important modifications include additional moment control and the use of encoders on the actuator-line-pulleys.

2.2 Configuration

Force allocation In this section two coordinates frames are used: $\{n\}$ is the local Earth-fixed basin frame defined in x,y and z direction, assumed inertial, while $\{b\}$ is the moving coordinate system fixed to the vessel body. Transformation from $\{n\}$ to $\{b\}$ is performed using the

rotation matrix $\boldsymbol{R}(\boldsymbol{\Theta})$, parameterized by the attitude vector $\boldsymbol{\Theta} = [\phi, \theta, \psi]^T$. See Fossen (2011). Unless otherwise specified, vectors in this paper are in $\{n\}$.

The position of end-effector i, denoted (x_{ei}, y_{ei}, z_{ei}), is given by

$$\begin{bmatrix} x_{ei} \\ y_{ei} \\ z_{ei} \end{bmatrix} = \boldsymbol{R}(\boldsymbol{\Theta}) \underbrace{\begin{bmatrix} x^b_{li} \\ y^b_{li} \\ z^b_{li} \end{bmatrix}}_{\boldsymbol{x_{li}}} + \underbrace{\begin{bmatrix} x \\ y \\ z \end{bmatrix}}_{\boldsymbol{\eta}} \tag{2}$$

where (x, y, z) is the position of the barge body frame in $\{n\}$ and $(x^b_{li}, y^b_{li}, z^b_{li})$ is the local lever arm to end effector i in $\{b\}$.

The position of the point where the actuator-line connects to the actuator-pulley i is (x_{ai}, y_{ai}, z_{ai}). The relative distance between end-effector and actuator is then

$$\Delta x_i = x_{ai} - x_{ei},\ \Delta y_i = y_{ai} - y_{ei}, \Delta z_i = z_{ai} - z_{ei} \tag{3}$$

The forces in x, y and z direction of line i now becomes:

$$[F_{x,i} \quad F_{y,i} \quad F_{z,i}]^T = \left(\frac{F_i}{R_i}\right) [\Delta x_i \quad \Delta y_i \quad \Delta z_i]^T, \tag{4}$$

where $R_i = \sqrt{\Delta x_i^2 + \Delta y_i^2 + \Delta z_i^2}$ is the line length of actuator i .

We aim at controlling the force in the three degrees of freedom of surge, sway, and yaw (i.e., position and heading). The force components induced in the other degrees of freedom are assumed negligible. The global load vector $\boldsymbol{F} = [F_x, F_y, M_\psi]^T$ for n actuation lines is a function of the individual line forces according to

$$\boldsymbol{F} = \underbrace{\begin{bmatrix} \frac{\Delta x_1}{R_1} & \frac{\Delta x_2}{R_2} & \dots & \frac{\Delta x_n}{R_n} \\ \frac{\Delta y_1}{R_1} & \frac{\Delta y_2}{R_2} & \dots & \frac{\Delta y_n}{R_n} \\ \frac{\Delta y_1 r_{x1} - \Delta x_1 r_{y1}}{R_1} & \frac{\Delta y_2 r_{x2} - \Delta x_2 r_{y2}}{R_2} & \dots & \frac{\Delta y_n r_{xn} - \Delta x_n r_{yn}}{R_N} \end{bmatrix}}_{\boldsymbol{T}} \underbrace{\begin{bmatrix} F_1 \\ F_2 \\ \vdots \\ F_N \end{bmatrix}}_{\boldsymbol{F}_l}, \tag{5}$$

where $r_{xi}{=}x_{ei}{-}x$ and $r_{yi}{=}y_{ei}{-}y$ are the lever arms in $\{n\}$.

Equation (5) can be used to find the desired line tensions $\boldsymbol{F}_l$, given a global target force $\boldsymbol{F}_t$. It is generally subject to constraints, such as a minimum and maximum tension. The studied system was sufficiently actuated by using the pseudoinverse (about the desired pretension line forces) to find a least squares values for $\boldsymbol{F}_l$, without violating these constraints.

Hydrodynamic Parameter Estimation The hybrid test setup was also used to identify the hydrodynamic properties of the vessel. A simplified vessels model in free decay is:

$$(M_A{+}M_{rb})\ddot{x}{+}D_q\dot{x}|\dot{x}|{+}D_l\dot{x}{=}F \tag{6}$$

wherein the performed decay tests, F is given by (1), under the assumption of perfect actuation and $\boldsymbol{\omega}{=}0$.

Faltinsen (1993, p. 252), suggests a method for estimating the nonlinear decay. However, identifying the nonlinear decay term was not found feasible for the given case.

Assuming only linear damping (setting $D_q{=}0$), the motions of a decay test can be described as a damped sine wave. The amplitudes, which are the data-points we wish to fit the experimental data to, can be expressed as:

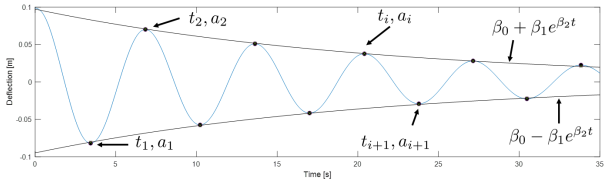

Fig. 4. Identification of decay-rate from decay tests.

$$\beta_0{+}Sign(\mathrm{a}_i)\beta_1 e^{\beta_2 t}, \tag{7}$$

where β_0 is the offset from the circular reference position caused by biases in the experimental setup, β_1 is the initial offset, β_2 is the decay rate of the system, and a_i is the amplitude, alternating between positive and negative.

Hydrodynamic parameters can then be extracted by:

$$\begin{aligned} T&{=}\frac{2(t_n{-}t_0)}{n} & w_d&{=}\frac{2\pi}{T} \\ M&{=}\frac{K}{w_d^2{+}\beta_2^2} & D&{=}{-}2M\beta_2 \end{aligned} \tag{8}$$

where $M{=}M_a{+}M_{rb}$ includes added mass and β_2 is found using an NLP-solver to minimise least square error of (7) onto the amplitudes from each test points; see Figure 4.

3. ANALYSIS

The experiments presented in this paper are all from decay-tests in still water, where the floating barge is released from an initial offset, and allowed to decay to its equilibrium point.

3.1 Target-Force Tracking Errors

We are not able to perfectly track the desired target-forces that are output from the numerical substructure. This causes an error which in Figure 5a can be recognized as the difference between the target and measured force.

Figure 5b illustrates how such errors affect the system in a decay test in sway-direction, and how the effect accumulates. The power-error seen in the figure was estimated by multiplying the end-effector velocity by the force-error of each actuator line, and the estimated energy-error is the power integrated with respect to time. In addition to lower frequency oscillations, three force error components are evident: 1) a high-frequency measurement noise component present at about 50 Hz, 2) large error amplitudes when the velocity changes direction, and 3) the applied force is, on average, ahead of the desired force (possibly due to overcompensation of delay).

Of the three mentioned issues, the first has little effect on the dynamics, since the noise frequency is much higher than the system eigenfrequency. The dynamic effect of the second is hypothesized to be reduced by the low power errors associated with the low velocity. The last issue is the most problematic, as it is continuously damping energy from the system.

The mean-average force tracking errors for decay tests with varying mooring stiffness are presented in Figure 6. The overall force tracking errors in these tests can be characterized as low. The figures also show good repeatability in that there are low variations within each test type.

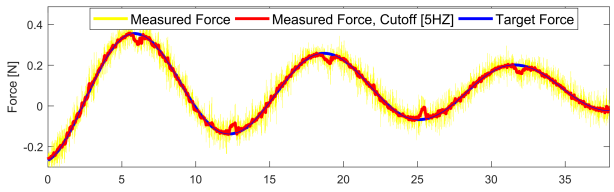

(a) Target versus measured force.

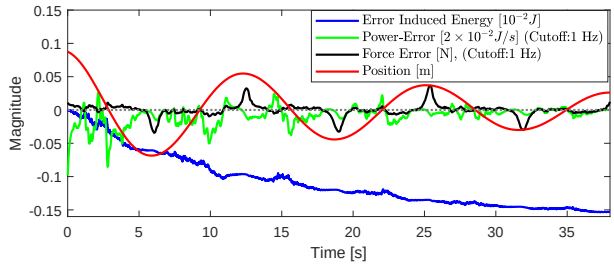

(b) Test data.

Fig. 5. Trajectory and errors for decay-test in x-direction. (k_x=$4N/m$)

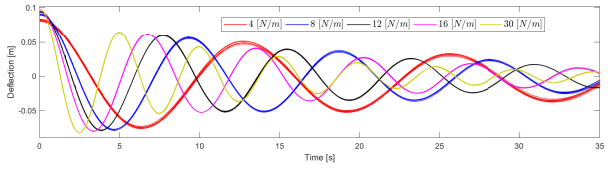

(a) Motions.

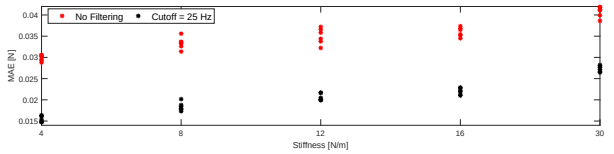

(b) Mean average force tracking error as function of stiffness.

Fig. 6. Trajectories (a) and mean-average force tracking errors (b) for decay tests in x-direction with varying numerical mooring stiffness.

Generally, experimental factors such as actuator dynamics, together with imperfections in the communication flow between the actuator and the real-time control-system will affect the applied forces and cause systematic errors that can accumulate over time if not properly handled. The tracking force errors occurring around velocity direction change, which was due to slack between transmission gears between the actuators and the encoders, serves as an example of this (this was later fixed).

Steps that can be taken to improve force tracking include improvements in communication flow (to reduce delays and jitter), improvements of the actuators (to reduce the effect of actuator dynamics), compensation of delays and dynamics, and better control design (to increase the responsiveness to more accurately track the target forces).

3.2 Force Allocation Errors

The accuracy of force allocation as given by (5), depends on how accurately we estimate the relative distances of (3). Here we separate between three types of errors. In the following, for a quantity κ, the estimation error is denoted $\delta_{(\kappa)}$=$\hat{\kappa}-\kappa$, (i.e., the estimated value minus the true value):

(1) Error in position estimate of the vessel ($\boldsymbol{\eta}$ and $\boldsymbol{\Theta}$): (δ_x,δ_y,δ_z,δ_ϕ,δ_θ,δ_ψ). This is a result of errors in the position tracking system, as well as errors induced when calibrating the vessel in the basin frame with respect to the markers on the vessel. These are reduced by a high quality tracking system, and precise alignment of the vessel in the basin frame.
(2) Error in actuator positioning ($\boldsymbol{x}_{ia}$): (δ_{xai},δ_{yai},δ_{zai}). As these are defined in the basin frame, it is important to know accurately how the basin coordinate frame is aligned relative to the basin walls.
(3) Error in lever arm estimation ($\boldsymbol{x_{li}}$): (δ_{xli},δ_{yli},δ_{zli}). These errors are relative to the body frame, and expected to be relatively simple to keep low.

The linearized error on the global force, given tension F_i in actuator i, and small errors $\boldsymbol{\delta}_\kappa$ is obtained by multiplying the resulting perturbations ($\delta_{\Delta xi}$,$\delta_{\Delta yi}$, $\delta_{\Delta zi}$) with the derivative of (4) with respect to Δx,Δy, and Δz:

$$\begin{bmatrix}\delta F_x\\ \delta F_y\\ \delta F_z\end{bmatrix}\Bigg|_{\delta=0} = \frac{1}{R_i^3}\begin{bmatrix}\left(\Delta y_i^2+\Delta z_i^2\right) & -(\Delta x_i \Delta y_i) & -(\Delta x_i \Delta z_i)\\ -(\Delta x_i \Delta y_i) & \left(\Delta x_i^2+\Delta z_i^2\right) & -(\Delta y_i \Delta z_i)\\ -(\Delta x_i \Delta z_i) & -(\Delta y_i \Delta z_i) & \left(\Delta y_i^2+\Delta z_i^2\right)\end{bmatrix}\begin{bmatrix}\delta_{\Delta xi}\\ \delta_{\Delta yi}\\ \delta_{\Delta zi}\end{bmatrix}\Big[F_i\Big], \tag{9}$$

where,

$$\begin{bmatrix}\delta_{\Delta x}\\ \delta_{\Delta y}\\ \delta_{\Delta z}\end{bmatrix} = \begin{bmatrix}\delta_x-\delta_{xai}\\ \delta_y-\delta_{yai}\\ \delta_z-\delta_{zai}\end{bmatrix}+\Big[R(\Theta)\Big]\begin{bmatrix}\delta_{xli}\\ \delta_{yli}\\ \delta_{zli}\end{bmatrix}+\begin{bmatrix}0 & r_{zi} & -r_{yi}\\ -r_{zi} & 0 & r_{xi}\\ r_{yi} & -r_{xi} & 0\end{bmatrix}\begin{bmatrix}\delta_\phi\\ \delta_\theta\\ \delta_\psi\end{bmatrix} \tag{10}$$

Using (10) it can further be shown that the linearized absolute force allocation error is bounded by:

$$\|\delta \boldsymbol{F_i}\| \leq \frac{1}{R_i}\|\delta\Delta\boldsymbol{x}\|F_{li}, \tag{11}$$

where $\|\delta\Delta\boldsymbol{x}\|$ is the euclidean norm of $[\Delta x,\Delta y,\Delta z]^T$.

From (9)-(11) it is clear that allocation errors due to inaccurate estimation of distances reduce rapidly with increased length of the actuator lines. Thus, not surprising, actuators placed far from the structure is much more robust in terms of avoiding allocation errors.

For the reviewed setup, a rough estimate suggests that the estimation errors of $\boldsymbol{\eta}$, $\boldsymbol{x}_{li}$, and $\boldsymbol{x}_{ia}$ are lower than 2cm, 0.5cm and 5cm, respectively, in any direction, while δ_ψ is estimated to be lower than two degrees. Using (9) on the resulting trajectories from the experimental data, it was estimated (always using the sign that increase errors), that in worst case, maximal decomposition error, of a line force F_i was lower than $0.032F_i[N]$ and $0.017F_i[N]$ in x- and y-direction, respectively.

Other sources of errors relating to force-allocation include basin coordinate system inaccuracies, deflection of actuator lines, and delayed measurements. For the presented tests, a guide was needed to ensure that the line stayed on the actuator pulley, resulting in some deflection of the line, causing minor additional decomposition errors.

In the presented case, the test-setup was installed in the laboratory for this particular testing campaign. It is expected that larger basin facilities, combined with standardized and careful positioning of actuators can reduce decomposition errors to an insignificant level.

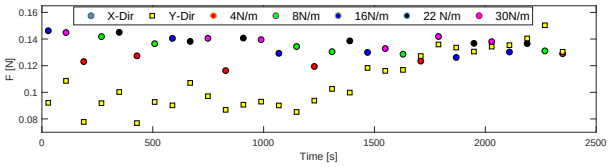

Fig. 7. Estimated bias. Samples were taken at start of each decay test in Figure 6(a). The tests were run consecutively without recalibrating

3.3 Force-Estimation Errors

As the estimated forces are used in feedback when applying target-forces on the physical substructure, any inaccuracies in the estimates will affect the applied forces.

The forces are measured by strain-gauge cells connecting the actuator lines to the physical substructure. Two types of errors are associated with these measurements: systematic errors and random errors.

Random Errors These are noise on the measurements signal, which can be identified in the steady state when vibrations have died out. Noting that the high-frequency oscillations observed in Figure 5(a) are mostly due to vibrations of the actuator interface, the observed random errors are small.

Systematic Errors These are bias-like errors between the measured and real force, typically caused by inaccurate (or no longer valid) calibrations and sensor drift (dominated by temperature-dependent drift). As opposed to the high-frequency random errors (which are filtered out), the effect of biases on the dynamics of the test-structure typically accumulates over time.

In the performed testing, the following measures were taken to reduce the systematic force measurement errors:

(1) Force sensors were routinely re-calibrated to zero.
(2) In the initialisation phase, a high linear stiffness was applied using the numerical substructure, forcing the vessel to the origin. When the system was stabilized at the pre-tensioned equilibrium point, the force sensors were resynchronized, ensuring minimal relative biases between the force-sensors.

The estimated applied force acting on the vessel before releasing the barge at the start of the tests of Figure 6(a) was recorded and is presented in Figure 7. As the vessel at this point is at rest, we know that the sum of forces should be zero. Thus, these forces provide an estimate of the systematic errors in the given configuration as they evolve over time. In retrospect, given the small dimensions of setup, the described procedure of re-synchronization could have been performed more often to reduce the systematic errors.

Both biases and random noise is to some degree independent of the magnitude of the applied forces. Thus, testing using larger scales and forces is expected to result in a relatively lower effect of biases and noise.

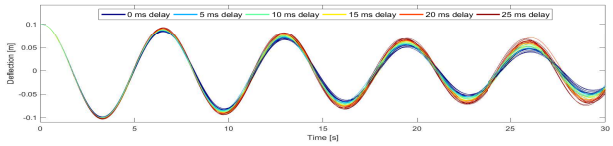

(a) Trajectories for varying added delay.

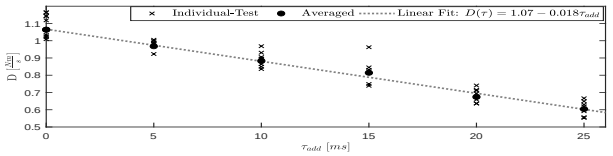

(b) Damping fitted to linear polynomial.

Fig. 8. Effect of added delay on decay test in surge direction. (k_y=16N/m)

3.4 Delay-Induced Force Errors

Due to communication delays, sampling, and processing time, there is a delay between the actual states of the system (which are measured inputs to the numerical substructure), and. This means that the forces we are tracking, in reality, are delayed relative to the ideal forces.

Theoretically, the instantaneous effect of a delay of a linear stiffness term, given sufficiently small delays, is the introduction of a negative linear damping coefficient proportional to the stiffness (Ueland and Skjetne, 2017):

$$D_{\text{induced}} = -K\tau, \tag{12}$$

where K is a linear stiffness coefficient, and τ is the delay between the actuated and ideal force.

The force delays were not known accurately for the test-case (but roughly estimated to be about 15 ms). In order to assess their effect, decay tests were performed where an extra delay was added to the target forces.

Figure 8(a) shows the resulting trajectories for introduced added delay ranging from 0 to 5 samples (0 to 25 ms) in decay in y-direction, with stiffness of k_y=16$\frac{N}{m}$. Although some internal variations between test sets are present, it is clear that the added delay introduces negative damping to the system.

The amplitudes are now fitted to (7) and (8), and subsequently fitted to a linear polynomial as a function of added delay. See Figure 8(b). It was hypothesised that we might observe a similar trend as (12); however, due to the presence of nonlinearities, test-variance, and imperfect actuation we should not expect an exact match to the instantaneous effect. The experimentally estimated, induced negative delay coefficient is found to be 18.8$\frac{N}{s}$ As such the experimental data are according to the expected trend.

As delays may have a profound effect on the system, it is advised to take measures to counteract it. For small delays, extrapolating data using least-square regression is found to be an effective countermeasure. See for example Wallace et al. (2005). The challenge is that it is difficult to estimate the delays accurately. Time-stamping measurement data, in a synchronised setup, is one means of obtaining delay estimates.

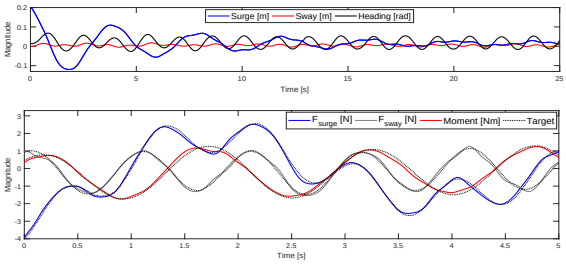

(a) $w0$=1.1 Hz

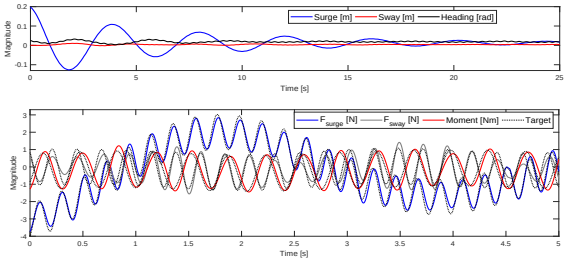

(b) w_0=4.8 Hz

Fig. 9. Decay tests in x-direction. Excitation force defined by(13) using $[k_x,k_y,k_\psi]$=$[16\frac{N}{m},30\frac{N}{M},12\frac{Nm}{rad}]$

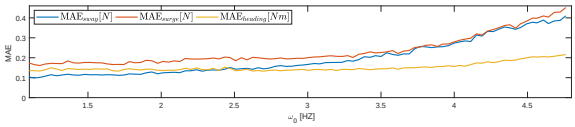

Fig. 10. Mean average force tracking error as function of excitation frequency.

4. TEST SETUP DISCUSSION

We have now illustrated issues that may affect the force actuation accuracy in a hybrid test setup. In this section, the test-setup, and its performance is further explored.

To demonstrate the flexibility of the setup, decay tests of the moored barge was combined with the introduction of numerically calculated harmonic forces. In these test, the additional external forces, to be actuated by the control system were given by:

$$\boldsymbol{w}=\left[\sin(2\pi w_0 t+\phi_1)\ \sin(1.8\pi w_0 t+\phi_2)\ \sin(1.2\pi w_0 t+\phi_3)\right]^T, \quad (13)$$

where the phase angles ϕ_i may vary from test to test.

In Figure 4 the resulting response and the systems ability to apply forces are shown for two cases of w_0. Figure 10 illustrates how the mean average error of the target tracking errors increases with the frequency of the harmonic force. Although the error increases with frequency, the tests indicate that the system was able to apply forces and moments quite well.

5. CONCLUDING REMARKS AND FURTHER WORK

In this paper we have, using a hybrid test setup, identified and discussed four sources of errors that affect the applied force from the ideal, non-sub-structured setup. Reducing these errors is of importance in ensuring realistic emulation of the original test case. Overall, testing shows promising potential of the method in the application to ship-shaped vessels.

Fig. 11. Test setup used on model-scale vessel.

In addition to response identification, hybrid testing of a moored vessel opens up for a wide arrange of flexible test opportunities. This may for example be relevant if the goal is to verify a DP-system, or snap loads in the mooring lines. The possibility of rapid changes and prototyping of the numerical substructure further means that tests can be performed in an efficient manner.

Future plans include a more in-depth review of the issues presented in this paper and the use a similar test-setup for identification of responses on a realistic model scenario. This may involve scaling considerations, more sophisticated numerical models, and a series of realistic waves spectrums. Figure 11 provides an image from initial testing.

REFERENCES

Cao, Y. and Tahchiev, G. (2013). A study on an active hybrid decomposed mooring system for model testing in ocean basin for offshore platforms. In *ASME 2013 32nd International Conference on Ocean, Offshore and Arctic Engineering*.

Carrion, J.E. (2007). *Model-based strategies for real-time hybrid testing*. University of Illinois at Urbana-Champaign.

Faltinsen, O. (1993). *Sea loads on ships and offshore structures*, volume 1. Cambridge university press.

Fossen, T.I. (2011). *Handbook of marine craft hydrodynamics and motion control*. John Wiley & Sons.

Sauder, T., Marelli, S., Larsen, K., and Sørensen, A.J. (2018). Active truncation of slender marine structures: Influence of the control system on fidelity. *Applied Ocean Research*, 74, 154–169.

Stansberg, C.T., Ormberg, H., and Oritsland, O. (2002). Challenges in deep water experiments: hybrid approach. *Journal of Offshore Mechanics and Arctic Engineering*, 124(2), 90–96.

Ueland, E.S. and Skjetne, R. (2017). Effect of time delays and sampling in force actuated real-time hybrid testing; a case study. In *OCEANS–Anchorage, 2017*, 1–10. IEEE.

Vilsen, S., Sauder, T., Sørensen, A.J., and Føre, M. (2018). Method for real-time hybrid model testing of ocean structures: Case study on horizontal mooring systems. *Submitted for Publication, January 2018*.

Vilsen, S.A., Sauder, T., and Sørensen, A.J. (2017). Real-time hybrid model testing of moored floating structures using nonlinear finite element simulations. In *Dynamics of Coupled Structures, Volume 4*, 79–92. Springer.

Wallace, M., Wagg, D., and Neild, S. (2005). An adaptive polynomial based forward prediction algorithm for multi-actuator real-time dynamic substructuring. In *Proceedings of the Royal Society of London A: Mathematical, Physical and Engineering Sciences*, volume 461.